Absence of chromosome axis protein recruitment prevents meiotic recombination chromosome-wide in the budding yeast Lachancea kluyveri

Sylvain Legrand, Asma Saifudeen, Hélène Bordelet, Julien Vernerey, Arnaud Guille, Amaury Bignaud, Agnès Thierry, Laurent Acquaviva, Maxime Gaudin, Aurore Sanchez, et al.

PNAS RESEARCH ARTICLE | GENETICS

Absence of chromosome axis protein recruitment prevents meiotic recombination chromosome-wide in the budding yeast *Lachancea kluyveri*

Sylvain Legrand[a,1,2], Asma Saifudeen[a,1], Hélène Bordelet[b], Julien Vernerey[a], Arnaud Guille[a], Amaury Bignaud[b], Agnès Thierry[b], Laurent Acquaviva[a], Maxime Gaudin[a], Aurore Sanchez[c], Dominic Johnson[d], Anne Friedrich[e], Joseph Schacherer[e], Matthew J. Neale[d], Valérie Borde[c], Romain Koszul[b], and Bertrand Llorente[a,2]

Edited by Michael Lichten, NIH, Bethesda, MD; received July 26, 2023; accepted January 24, 2024

Meiotic recombination shows broad variations across species and along chromosomes and is often suppressed at and around genomic regions determining sexual compatibility such as mating type loci in fungi. Here, we show that the absence of Spo11-DSBs and meiotic recombination on Lakl0C-left, the chromosome arm containing the sex locus of the *Lachancea kluyveri* budding yeast, results from the absence of recruitment of the two chromosome axis proteins Red1 and Hop1, essential for proper Spo11-DSBs formation. Furthermore, cytological observation of spread pachytene meiotic chromosomes reveals that Lakl0C-left does not undergo synapsis. However, we show that the behavior of Lakl0C-left is independent of its particularly early replication timing and is not accompanied by any peculiar chromosome structure as detectable by Hi-C in this yet poorly studied yeast. Finally, we observed an accumulation of heterozygous mutations on Lakl0C-left and a sexual dimorphism of the haploid meiotic offspring, supporting a direct effect of this absence of meiotic recombination on *L. kluyveri* genome evolution and fitness. Because suppression of meiotic recombination on sex chromosomes is widely observed across eukaryotes, the mechanism for recombination suppression described here may apply to other species, with the potential to impact sex chromosome evolution.

meiosis | homologous recombination | yeast | genetics | genome

DNA double-strand breaks (DSBs) initiate recombination between homologous chromosomes during meiotic prophase, an important event that promotes chromosome segregation, and hence fertility and genome evolution (1–3). The type II topoisomerase–related protein Spo11 is the catalytic subunit of a multiprotein machinery that generates the meiotic DSBs (4–8). Such Spo11-DSBs occur within nucleosome-free DNA, typically found in gene promoters that constitute Spo11-DSB hotspots in the yeast model *Saccharomyces cerevisiae* (9–11). The Spo11-DSB hotspot landscape is relatively well conserved among *Saccharomyces* species, likely because gene promoters are conserved functional elements that are under selective constraints (12).

In *S. cerevisiae,* meiotic prophase chromosomes undergo compaction to form chromatin loops of ca. 20 to 100 kb (13–18). These chromatin loops are anchored on a protein axis composed of a coalescence of cohesins, the axis-core protein Red1, and the HORMA domain-containing protein Hop1 (19–22). The current model of axis proteins recruitment is that the meiotic specific kleisin cohesin subunit Rec8 ensures most of Red1 recruitment through direct interaction, and that Red1 then recruits its interacting partner, Hop1 (16, 23). A second parallel pathway relies on a direct Hop1-chromatin interaction within broad genomic islands with high gene density, leading to further recruitment of Red1 (24). Spo11-DSB hotspots are specifically located within chromatin loops, away from the chromosome axis attachment sites at the base of these loops (16). While Rec8 is dispensable for Spo11-DSBs, the absence of either Red1 or Hop1 strongly reduces Spo11-DSBs, notably because Hop1 participates in the recruitment of Mer2, a key Spo11 cofactor for DSB formation (16, 25–32).

After DNA cleavage, Spo11 is released from DNA ends by the Mre11/Rad50/Xrs2 complex in combination with Sae2 but remains covalently attached to an oligonucleotide (33, 34). Spo11-oligo sequencing allowed the establishment of a nucleotide-level resolution Spo11-DSBs genome-wide map (10). Once processed, Spo11-DSBs are primarily repaired by homologous recombination with the non-sister homologous chromatids, to eventually yield crossovers (35, 36). This promotes pairing and synapsis of the homologous chromosomes through the synaptonemal complex assembly. The main component of this proteinaceous complex is the transverse filament protein Zip1, and its lateral elements

Significance

Meiosis is the specialized cell division generating gametes. In most organisms including the extensively studied yeast *Saccharomyces cerevisiae*, parental homologous chromosomes recombine during meiosis prophase which ensures proper chromosome segregation and shuffles parental genetic information. While recombination is generally suppressed at sex loci, such suppression sometimes extends over entire chromosome arms by unknown mechanisms. Using the poorly studied yeast *Lachancea kluyveri*, a *S. cerevisiae* relative, we show that recombination suppression can be mediated over the entire chromosome arm containing the sex locus by the absence of recruitment of proteins essential for recombination initiation. This novel mechanism for recombination suppression affects *L. kluyveri* genome evolution and fitness, and may apply to other species, with the potential to impact sex chromosome evolution.

The authors declare no competing interest.

This article is a PNAS Direct Submission.

[1]S.L. and A. Saifudeen contributed equally to this work.

[2]To whom correspondence may be addressed. Email: sq.legrand@outlook.com or bertrand.llorente@inserm.fr.

This article contains supporting information online at https://www.pnas.org/lookup/suppl/doi:10.1073/pnas.2312820121/-/DCSupplemental.

Published March 13, 2024.

correspond to the chromosome axes (37). The chromosome axis component Hop1 is eventually removed from the axis upon completion of synaptonemal complex formation, shutting down DSB formation (21, 38–40). Interestingly, the length of the synaptonemal complex covaries with the number of crossovers independently of the genome size and the species (41, 42). In *S. cerevisiae*, the major crossover formation pathway involves the ZMM proteins (Zip1, 2, 3 and 4; Spo16; Msh4 and 5; and Mer3 (43, 44). Zip3 appears as a specific marker of the resulting "type I" crossovers that show interference (45, 46). Genome-wide distribution of Zip3 colocalizes with Spo11-DSBs and alternates with chromosome axis binding sites (46, 47).

Meiotic homologous recombination is commonly repressed around the loci determining sexual compatibility such as the mating-type loci in fungi, and sometimes this inhibition extends outside of this locus (48). Both the mechanism and the selective advantage of recombination suppression are unclear. Recombination inhibition within the *MAT* locus may prevent loss of heterozygosity at this specific locus and subsequent disequilibrium between the two mating types within the population. In addition, recombination inhibition around the *MAT* locus may ensure linkage between specific alleles that present strong selective advantages when linked (49). As another example of recombination inhibition around the mating-type locus, we previously reported a complete inhibition of meiotic recombination over almost the entire chromosome arm containing the mating type locus of the budding yeast *Lachancea kluyveri* (50). The inhibition spreads over the region of the left arm of *L. kluyveri* chromosome C starting from the left telomere to a point about 10 kb to the left of the centromere; we refer to this region as Lakl0C-left. This inhibition of recombination results from the repression of Spo11-DSBs within this ca. 1 Mb long region, corresponding to ca. 8% of *L. kluyveri* genome. So far, the mechanism inhibiting Spo11-DSB formation over such a large genomic region is unknown.

L. kluyveri is a *Saccharomycetaceae* yeast that diverged from *S. cerevisiae* prior the whole genome duplication that characterizes the *Saccharomyces* lineage (51). *L. kluyveri* has only eight chromosomes, with a genome size and a gene complement comparable to *S. cerevisiae* (52, 53). As in *S. cerevisiae*, meiosis is efficiently induced by nitrogen starvation and meiotic progression is rather synchronous (50). Interestingly, Lakl0C-left is characterized by a G + C frequency 12% higher than the rest of the genome (53). A population genomics survey of *L. kluyveri* led to the proposal that Lakl0C-left arose from an introgression from a yet unknown *Lachancea* species (54). Finally, Lakl0C-left contains almost exclusively early replication origins, in contrast to the rest of the genome (55). Whether any of these Lakl0C-left specificities are at the source of the repression of Spo11-DSBs formation is unknown.

Here, we confirm Spo11-DSB inhibition on Lakl0C-left using a genome-wide DSB mapping method (56) and find that the Spo11-DSB hotspot landscape shows some conservation between orthologous syntenic intergenic regions from *L. kluyveri* and *S. cerevisiae*. Using Hi-C, we showed that *L. kluyveri* chromosomes undergo compaction during meiotic prophase, and that Lakl0C-left compaction is comparable to the rest of the genome, which correlates with a comparable binding of Rec8 as detected by ChIP-seq. By contrast, Hop1 and Red1 are completely absent from Lakl0C-left, likely explaining the lack of Spo11-DSBs. Finally, fluorescence visualization of Zip1, Rec8 and the left and right arms of chromosome C recapitulated these molecular findings and revealed the lack of pairing of Lakl0C-left. Overall, *L. kluyveri* chromosome C appears as a prototypical young sex chromosome.

Results

Genome-wide Spo11-DSB Mapping in *L. kluyveri*. Using pulsed-field gel electrophoresis (PFGE) and Southern blotting, we previously showed that Lakl0C-left is depleted of Spo11-DSBs but flanked by a Spo11-DSB hotspot in the *GPI18* promoter, located about 10 kb to the left of the centromere. We also identified by Southern blot two additional DSB hotspots in the promoters of the *RAS1* and *PIS1* genes that correlate with crossover hotspots (50). To confirm these results with an independent technique and to extend them to the whole genome, we used the Covalent Complexes-sequencing (CC-seq) technique that allows nucleotide-resolution mapping of protein-linked DNA breaks (56).

We performed two independent experiments. After background filtering (methods), we identified a specific signal that clustered into hotspots, as seen for *S. cerevisiae* Spo11-DSBs, and the two replicates showed good reproducibility (Fig. 1*A* and *SI Appendix*, Fig. S1). We used the MACS2 peak calling algorithm to define the Spo11-DSB hotspots (57). One replicate showed better signal enrichment than the other (1,933 hotspots vs. 1,025 hotspots, *SI Appendix*, Fig. S1) and was used for subsequent analyses.

The average DSB hotspot density is 1 per 5.9 kb and the average width is 0.282 kb in *L. kluyveri* compared to 1 per 4.2 kb and 0.409 kb, respectively in *S. cerevisiae* (56). As in *S. cerevisiae*, most DSB signal is in intergenic regions between divergent or tandemly orientated genes (Fig. 1*B* and *SI Appendix*, Fig. S2). Only 13.2% of the DSB signal is within genes and 3.1% is within intergenic regions between convergent genes. In addition, centromere-flanking regions, subtelomeres, and the rDNA locus were depleted for Spo11-DSBs compared to the rest of the genome (*SI Appendix*, Figs. S3 and S4). However, and in sharp contrast with the rest of the genome, a depletion of Spo11-DSBs was observed all along Lakl0C-left, which shows a 12-fold decrease in Spo11-DSBs per base pair compared to the rest of the genome (Fig. 1*A*). Overall, genome-wide mapping of Spo11-DSBs reveals similar properties of Spo11-DSBs distribution between *L. kluyveri* and *S. cerevisiae* chromosomes and confirms the depletion of Spo11-DSBs in Lakl0C-left.

Spo11-DSBs Hotspots Strength Is Rather Well Conserved between *L. kluyveri* and *S. cerevisiae*. Spo11-DSBs hotspot positions and strength are remarkably conserved within *Saccharomyces* species, likely because they are mainly found within gene promoters, which are functional genetic elements (12). In *L. kluyveri*, Spo11-DSBs are also mainly located within gene promoters. To test the conservation of Spo11-DSBs hotspot strength between *L. kluyveri* and *S. cerevisiae,* we compared Spo11-DSBs levels in syntenic intergenic regions (sIGRs), i.e., intergenic regions flanked by pairs of orthologous genes. Although these two species diverged over 100 Mya, they share 239 synteny blocks and 2,030 sIGRs (58). The Pearson correlation coefficient between the log2 transformed Spo11-DSB hotspots strength of the two species is r = 0.63 (P = 1.4e-220, 95%CI [0.61, 0.66]) (Fig. 2*A*), only slightly lower than the one observed within the *Saccharomyces* clade between *S. cerevisiae* and *S. kudriavzevii* (12).

To assess the conservation of Spo11-DSB hotspot strength on an evolutionary scale broader than that of the *Saccharomyces* species, but independently of *L. kluyveri*, we focused on ohnologs (59). These are the subset of *S. cerevisiae* paralogs that emanated from the whole genome duplication that characterizes the *Saccharomyces* lineage, but that occurred after the divergence between the *Saccharomyces* and the *Lachancea* lineages (60). We identified 39 sIGRs among the 547 ohnolog pairs. Considering

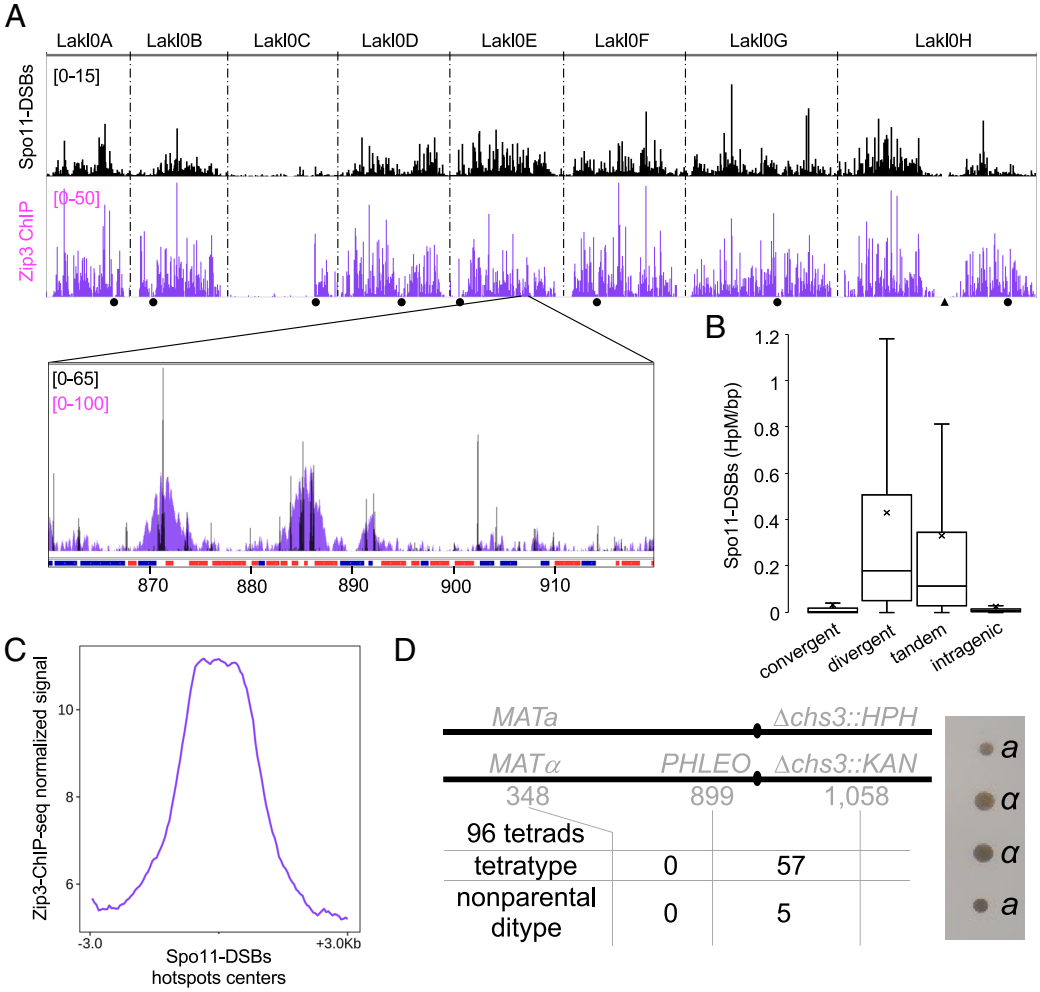

Fig. 1. LaklC-left is depleted in Spo11-DSBs, Zip3, and crossovers. (*A*) Genome-wide CC-seq (Spo11-DSBs, *Top*) and Zip3-FLAG ChIP-seq (*Bottom*) profiles of *L. kluyveri* CBS10367 at 6 h post meiosis induction. The eight chromosomes are concatenated in the alphabetical order from A (*Left*) to H (*Right*) and separated by vertical dotted lines. Black discs indicate centromeres. The black triangle indicates the rDNA locus position, which corresponding signal has been masked. The *y* axis of the CC-seq profile represents the Spo11-DSB count after denoising of a single experiment. The *y* axis of the Zip3-FLAG ChIP-seq profile represents the mean ChIP-seq signal of five independent experiments. A zoom in a representative region of chromosome E with superimposition of the CC-seq and Zip3-FLAG ChIP-seq signals is shown. Coding regions are represented on the *x* axis (chromosome coordinates in kilo bases). Transcription is left to right for red boxes and right to left for blue boxes. Maximum values are lower in the genomic view due to visualization constraints. (*B*) Box plot representing the distribution of the CC-seq signal according to the type of genomic location. Intergenic regions comprise regions flanked by convergent genes, divergent genes, and genes that are in a head-to-tail (tandem) configuration. Horizontal bars show the medians and crosses show the means. Boxes delimit the first and third quartiles. The error bars represent minimum and maximum values. (*C*) Average signals of five independent Zip3-FLAG ChIP-seq experiments performed 6 h after meiosis induction piled up around the centers of the 500 strongest Spo11-DSBs hotspots defined by MACS2 from the CC-seq experiment. (*D*) Recombination assay in the *L. kluyveri* CBS10367 diploid strain. The two copies of chromosome C are represented as a horizontal black line. Relevant loci are indicated as well as their chromosome coordinates in kb. *PHLEO* was integrated at the LaklC-899 locus. The black ovals represent centromeres. The table indicates single and double crossovers (CO) between *MAT* and *PHLEO* and between *PHLEO* and *CHS3* out of 96 tetrads. The picture on the right is representative of a full tetrad with the two *MATα* colonies exhibiting a smaller size than the two *MATα* colonies.

the Spo11-oligo data from ref. 10 corresponding to these 39 sIGRs, the Pearson correlation coefficient between the log2 transformed Spo11-DSB hotspots strength of these sIGRs is $r = 0.37$ ($P = 0.021$, 95%CI [0.06, 0.62]) (Fig. 2*B*). This shows that the strength of Spo11-DSBs associated to this subset of intergenic regions also exhibits some conservation over an evolutionary scale much broader than that of the *Saccharomyces* clade.

Overall, analysis of both orthologous syntenic IGRs and ohnologous syntenic IGRs revealed some conservation of Spo11-DSBs strength at an evolutionary scale broader than what has been reported so far (12).

Spo11-DSBs Sites Are Enriched in the Crossover Factor Zip3. In *S. cerevisiae*, the crossover factor Zip3 is enriched around Spo11-DSBs (46). To determine whether this is also the case in *L. kluyveri*, we performed ChIP-seq experiments using Zip3 FLAG-tagged on its carboxyl terminus as a bait. As in *S. cerevisiae*, Zip3 is specifically expressed after meiotic induction (*SI Appendix*, Fig. S5). We observed Zip3 ChIP-seq enrichment peaks genome-wide, with the notable exception of LaklC-left and about 250kb left and right of the rDNA locus on LaklH (Fig. 1*A* and *SI Appendix*, Fig. S4). Piling up Zip3 ChIP-seq signals centered on the 500 strongest Spo11-DSBs hotspots revealed a specific Zip3 enrichment around these Spo11-DSBs hotspots (Fig. 1*C*). Importantly, the absence of Zip3 ChIP-seq signal on LaklC-left suggests a complete absence of crossovers in this chromosome arm in the nearly homozygous CBS10367 strain background used here. This population average analysis confirms and generalizes our original observation suggesting, from a limited number of meioses in the artificial NBRC10955 x 67-588 hybrid background, a lack of recombination along this arm (50, 61).

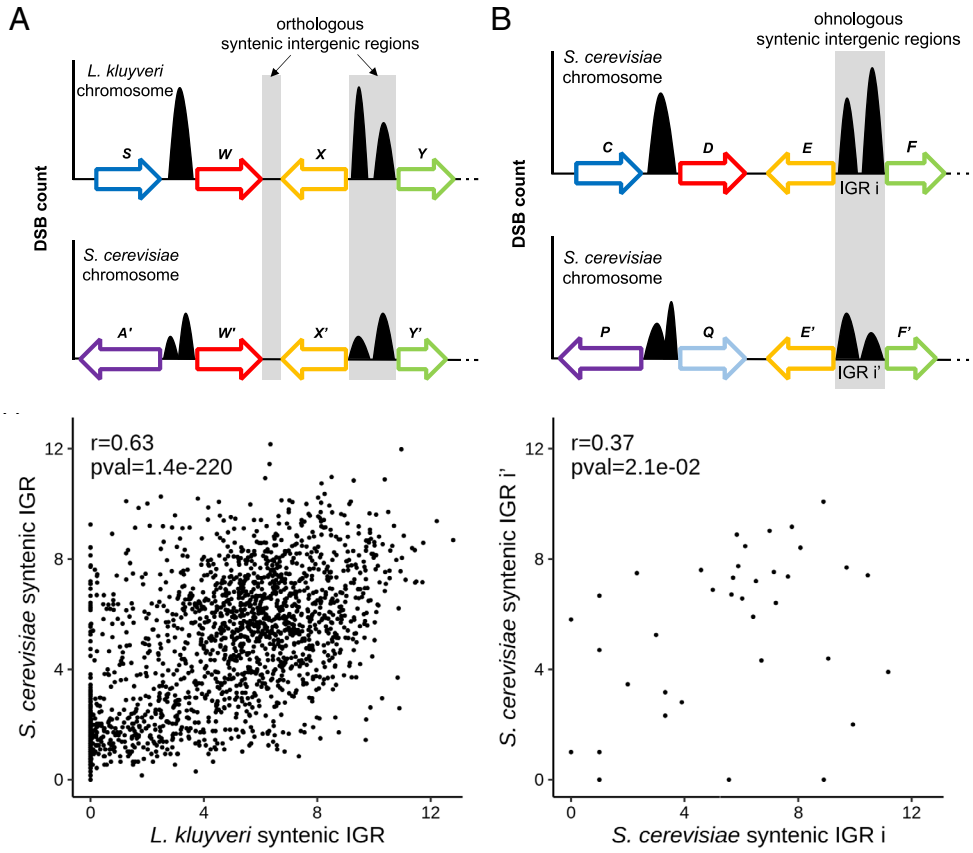

Fig. 2. Spo11-DSB signal conservation across syntenic intergenic regions (IGR) between *L. kluyveri* and *S. cerevisiae*, and between *S. cerevisiae* ohnologs. (*A*) *Top* panel represents syntenic intergenic regions (highlighted by gray boxes) in *L. kluyveri* and *S. cerevisiae* that are flanked by orthologous genes couples (W-W′, X-X′, and Y-Y′ are orthologous pairs while S-A′ is not). The bottom graph shows the comparison of the CC-seq Spo11-DSB signal from 1,956 syntenic IGR between *L. kluyveri* (*x* axis) and *S. cerevisiae* (*y* axis) with the Pearson correlation coefficient r indicated and the associated *P* value. Displayed data are log2 transformed counts to which a (+1) pseudo count has been added (log2(x + 1)) to avoid negative or infinite values. (*B*) Same as in *A* except that 39 *S. cerevisiae* intergenic regions flanked by couples of ohnologs are considered (E-E′ and F-F′ are pairs of ohnologs while C-P and D-Q are not).

The Lack of Meiotic Recombination on Lakl0C-left Is Conserved among *L. kluyveri* Isolates and Results in a *MAT*-linked Growth Phenotype. We attributed the complete absence of recombination on Lakl0C-left observed in a hybrid background to the strong depletion of Spo11-DSBs, as measured previously by Southern blot (50) and here by CC-seq in the natural CBS10367 diploid background (54). However, we cannot rule out that a low level of Spo11-DSBs would be enough to induce recombination within Lakl0C-left in this homozygous background, but not in a hybrid background, where sequence polymorphism would prevent recombination through the action of mismatch repair (62–64).

We therefore designed a reporter assay inserting drug resistance cassettes to monitor recombination within two intervals of *L. kluyveri* chromosome C in the nearly homozygous CBS10367 background (Fig. 1*D*). From left to right, the first interval is exclusively on Lakl0C-left and spans about 550 kb from *MAT* to the Lakl0C-899 locus positioned about 110 kb left of the centromere. The second interval starts from Lakl0C-899 to the *CHS3* locus located about 50 kb right of the centromere and is about 160 kb long. The spore viability of the resulting strain is 76% (n = 96 tetrads), similar to that of the parental strain (83%, n = 39 tetrads). From 96 tetrads with four viable spores, we did not detect a single crossover on the Lakl0C-left 550 kb long interval and we detected 57 single crossovers and five double crossovers on the second 160 kb long interval (Fig. 1*D*). The absence of recombinants on the Lakl0C-left interval in this nearly completely homozygous context shows that inter-homolog recombination is inhibited on Lakl0C-left independently of sequence polymorphism, and that the low Spo11-DSBs level detected does not promote recombination. The absence of meiotic recombination on Lakl0C-left therefore occurs in both the NBRC10955 x 67-588 hybrid and the CBS10367 strains. Given the *L. kluyveri* phylogeny (54), this shows that recombination cessation on Lakl0C-left is ancient and likely common to the entire population.

Remarkably, *MATa* colonies coming from CBS10367 spores were systematically smaller than *MATalpha* colonies (Fig. 1*D*). One explanation could be that there is at least one DNA sequence polymorphism between the *MATa* and *MATα*-associated linkage groups responsible for this sexual dimorphism in the CBS10367 natural diploid. This would agree with the fact that non-recombining regions tend to accumulate heterozygous DNA sequence polymorphisms, as frequently observed for sex chromosomes (ref. 48 and *Discussion*). Alternatively, differentially expressed genes between *MATa* and *MATalpha* cells could be responsible for this growth phenotype, although this is not the case in other species including *S. cerevisiae*.

Hi-C Reveals Similar Compaction Level of all *L. kluyveri* Meiotic Chromosomes. We wondered whether the lack of recombination on Lakl0C-left could result from a peculiar chromosome structure that would differ from the canonical compaction of chromosomes during meiosis prophase into cohesin-mediated chromatin loops (14). Using Hi-C (15, 65), we generated genome-wide contact maps of eight *L. kluyveri* meiotic timepoints harvested between 0 and 8 h after meiosis induction. ~70% of cells passed the second

meiotic division at the 8-h timepoint (*SI Appendix*, Fig. S6*A*). Overall, the contact maps of *L. kluyveri* meiotic Hi-C resemble those from *S. cerevisiae* (Fig. 3*A*) (15, 17). Centromere clustering is clearly visible at t = 0 (Rabl configuration) and is progressively lost (Fig. 3*A* and *SI Appendix*, Fig. S6B). Chromosomes gradually individualize, as shown by the increase and decrease of intra- and inter-chromosomal contacts, respectively. Compaction was maximal 5 h following entry into meiosis (*SI Appendix*, Fig. S6*C*). Enrichment in intrachromosomal contacts involves pairs of loci within the 10 to 200 kb range, as illustrated both by the thickening of the main diagonals on the normalized contact maps (Fig. 3 *A* and *B*) and the shoulder made by the distance law, reflecting the genomic average contact frequencies over increasing genomic distances (Fig. 3*C*). This compaction most likely results from the folding of chromatin into loops by the cohesin complex (15, 17, 18). Remarkably, the Hi-C pattern displayed by the Lakl0C-left was comparable to the other chromosomes. The intrachromosomal contact frequency and the distance law of the Lakl0C-left arm displayed nearly the same compaction throughout the meiotic time course than the other chromosome arms of similar lengths (Fig. 3*C* and *SI Appendix*, Fig. S6 *D* and *E*). In addition, based on similar interchromosomal contact frequencies compared to the other chromosome arms, Lak0C-left is not isolated from the other chromosomes (Fig. 3*A* and *SI Appendix*, Fig. S6 *C* and *D*). Overall, Lakl0C-left is folded into cohesin-mediated loops, whose scores, length and kinetic of formation are similar to loops analyzed on other chromosomal arms (Fig. 3 *B*, *D*, and *E* and *SI Appendix*, Fig. S6 *E* and *F*). In conclusion, this shows that the lack of

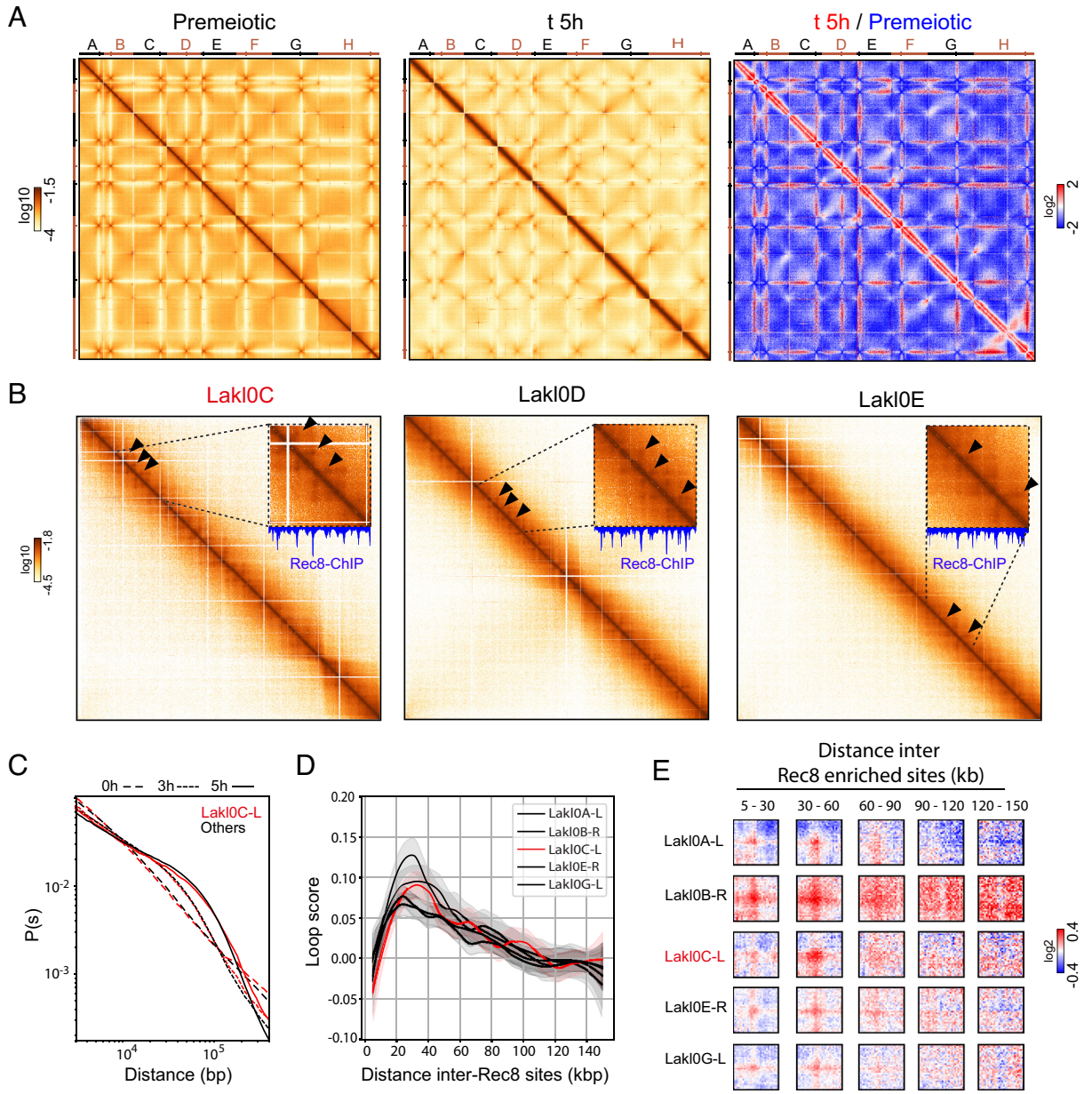

Fig. 3. Lakl0C-left compaction along meiotic prophase is similar to other chromosomal arms. (*A*) Contact maps of the whole genome of *L. kluyveri* before (*Left*) and 5 h (*Middle*) after induction of meiosis. Ratio maps of 5 h over premeiotic chromosomes (*Right*). Bin size, 10 kb. (*B*) Contact maps of chromosome C (*Left*), D (*Middle*), and E (*Right*) at 5 h after meiosis induction. Bin size, 1 kb. Magnified *Insets* show portions of 200 kb, with the corresponding Rec8 ChIP over untagged ratio profiles, determined at 4 h post meiosis induction. (*C*) Distance laws of Lakl0C-left compared to the mean of ~1 Mb of different chromosome arms before, 3 h and 5 h post meiosis induction. (*D*) Spectrum of loop score detected at 5 h post meiosis induction at the intersection of Rec8 peaks detected at 4 h post meiosis induction, as a function of the distance separating the pair of Rec8 peaks (kb). L and R refer to left and right arms, respectively. (*E*) Aggregated ratio maps of 29-kb windows (5 h post meiosis induction) centered on pairs of Rec8 peaks (4 h post meiosis induction) over randomly chosen positions in the same inter-distance range. Bin size: 1 kb.

recombination of Lakl0C-left is not associated with any specific structure detectable by Hi-C, and that Lakl0C-left undergoes similar compaction by cohesins as all other chromosomes.

Meiotic Axis Proteins Hop1 and Red1 Are Absent from Lakl0C-left. The compaction of Lakl0C-left suggests the loading of cohesins, including the meiosis-specific Rec8 kleisin subunit. To assess this, we performed ChIP-seq analysis of Rec8, FLAG-tagged at its carboxy terminus, which was specifically expressed after meiosis induction and show retarded forms on western blots, as in *S. cerevisiae* (*SI Appendix*, Fig. S5) (Brar et al. (66)). *L. kluyveri* Rec8 ChIP-seq profiles are similar to those of *S. cerevisiae* (Fig. 4). The Rec8 ChIP-seq signal first appears early (1 h) after induction of meiosis around all centromeres (*SI Appendix*, Fig. S7) (32). Four hours after meiosis induction, the Rec8 ChIP-seq signal is then distributed in peaks throughout the genome and accumulates in convergent intergenic regions, likely as a result of transcription (Fig. 4 and *SI Appendix*, Figs. S7 and S8 *A* and *B*) (23, 67). In addition, Rec8 ChIP-seq peaks alternate with the peaks of Zip3 ChIP-seq and Spo11-DSBs CC-seq (*SI Appendix*, Fig. S8 *A* and *C*). Such a distribution is compatible with the loop-axis structure of meiotic chromosomes, with Spo11-DSBs formed within the loops at the basis of which lie the axis proteins including Rec8 (16). Importantly, the loci at the basis of such chromatin loops detected as discrete dots away from the diagonal in the Hi-C experiments are enriched in Rec8 (Fig. 3 *B* and *E*) (68). Furthermore, Rec8 ChIP-seq signal is decreased in subtelomeric regions (*SI Appendix*, Figs. S4 and S9). We noted a slight reduction of Rec8 ChIP-seq signal on Lakl0C-left relative to the rest of the genome (*SI Appendix*, Fig. S8*B*, compare right and left panels, respectively). However, it comes from a nonspecific sequencing bias, also observed in the untagged control, that is likely due to the elevated GC content of Lakl0C-left (69). Considering this sequencing bias, the overall Lakl0C-left Rec8 ChIP-seq signal is comparable to the rest of the genome, which is in agreement with the Hi-C results showing comparable compactions.

Coalescence of cohesins participates in the formation of the chromosome axes that also comprise Hop1 and Red1, needed for Spo11-DSBs formation (26–28, 30, 31). Since Rec8 loads normally on Lakl0C-left, we investigated whether Red1 and Hop1 were also loaded. Like for Rec8, we tagged Red1 and Hop1 with FLAG at their carboxy termini. As in *S. cerevisiae*, both proteins are specifically expressed after meiosis induction and show retarded forms on western blots (*SI Appendix*, Fig. S5) (70, 71). In addition, Red1 and Hop1 ChIP-seq signals form peaks that strongly colocalize with Rec8 ChIP-seq peaks (Fig. 4 and *SI Appendix*, Figs. S7 and S8 *A* and *D*). However, several cases of Rec8 peaks without associated Hop1 or Red1 peaks were noted. First, Red1 and Hop1 are depleted around centromeres, unlike Rec8 (*SI Appendix*, Figs. S4, S9 and S10). This depletion of Red1 and Hop1 coincides with the depletion of the Spo11-DSB signal (Fig. 1*A* and *SI Appendix*, Figs. S3 and S8*A*) and the decrease in recombination (50), as seen in *S. cerevisiae*. Second, around the rDNA locus, while neither Rec8 nor Red1 ChIP-seq signal shows any decrease compared to the rest of the genome, the Hop1 ChIP-seq signal is decreased (*SI Appendix*, Figs. S4 and S9, chromosome H). Strikingly, this decrease occurs on a much narrower region than that of Zip3. Finally, the most remarkable discrepancy between Rec8 and Hop1/Red1 signal was observed on Lakl0C-left, where virtually no Red1 or Hop1 ChIP-seq signal was observed despite a normal Rec8 loading (Fig. 4). While in *S. cerevisiae* Hop1- and Red1- rich or poor regions have been described (16, 72), a complete depletion over an almost entire chromosome arm is observed in this study. Given the importance of Hop1 and Red1 for Spo11-DSBs formation, it is tempting to speculate that their absence is directly responsible for the absence of Spo11-DSBs formation on Lakl0C-left.

Spo11-DSBs Formation Inhibition on Lakl0C-left Is Independent of Tel1. In the absence of Tel1, Spo11-DSBs increase in *S. cerevisiae*, although to a lesser extent than what is observed in the absence of its ATM homolog in mice, notably on the non-homologous

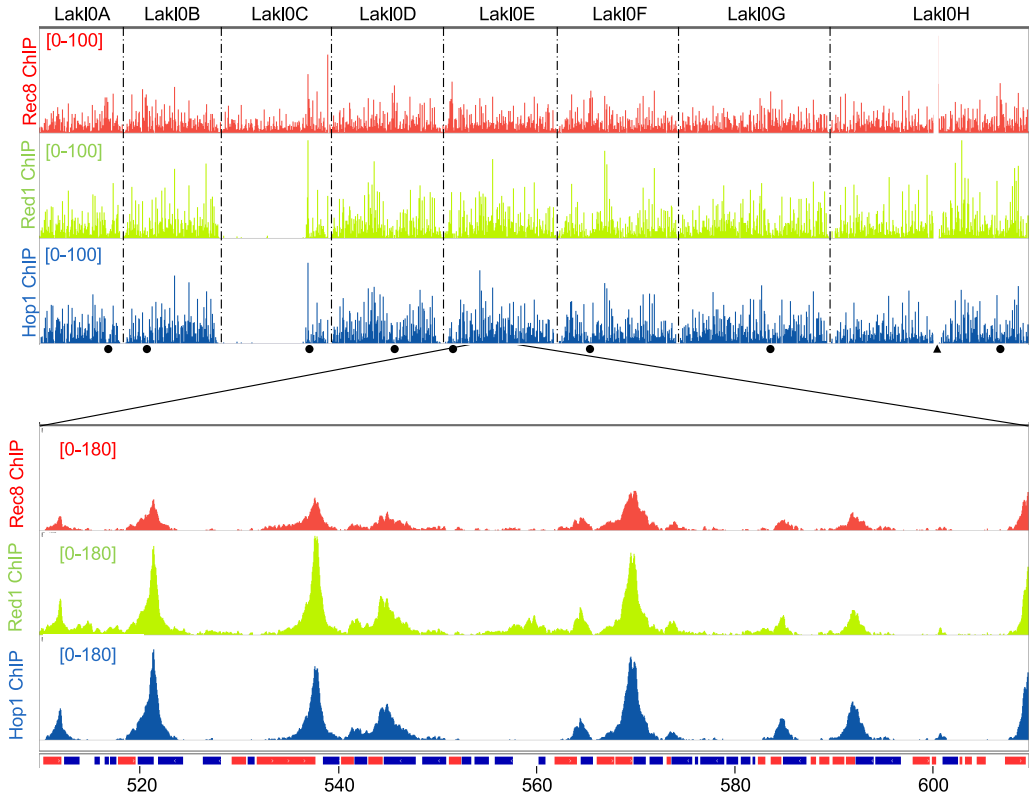

Fig. 4. ChIP-seq of chromosome axis proteins Rec8-FLAG, Hop1-FLAG, and Red1-FLAG. The *Top* panel represents the genome-wide ChIP-seq signals from two independent experiments 6 h after meiosis induction for the three proteins. Same legend as in Fig. 1. The *Bottom* panel is a close-up view of a representative genomic region of chromosome E illustrating the strong similarity between the ChIP-seq profiles of the three proteins. Genes coding regions are represented as in Fig. 1*A*.

parts of the sex chromosomes (73–75). We therefore tested by PFGE followed by Southern blot meiotic Spo11-DSBs formation in the *tel1* null mutant. The overall Spo11-DSB profile is similar in the reference and *tel1* backgrounds, notably on chromosome C (*SI Appendix*, Fig. S11). This shows that Spo11-DSB depletion on Lakl0C-left is independent of Tel1.

The Lack of Recombination on Lakl0C-left Is Independent of Its Early Replication Timing. Spo11-DSB formation is coordinated with meiotic DNA replication and occurs on fully replicated chromosomes (76–78). Interestingly, Lakl0C-left is replicated earlier than the rest of the genome due to the prevalence of early firing replication origins in vegetative cells (55, 79). Although studies in *S. cerevisiae* suggest that this would result in early recruitment of DSB factors and early DSB formation on Lakl0C-left (27, 78), we wondered whether, in *L. kluyveri*, early replication timing would prevent Spo11-DSBs formation, and hence recombination. Therefore, we subdivided the genome in four replication quartiles of 8 min each based on the known vegetative replication timing (55, 79) and assessed Spo11-DSBs and Zip3-ChIP-seq signals. This partitioning shows that the early replication quartile encompasses a smaller genomic fraction than the mid-early and the mid-late replication quartiles, but a larger genomic fraction than the late replication quartile (Fig. 5*A*). In addition, it shows that Lakl0C-left contains mainly early and mid-early replicated regions. Considering the genomic fraction encompassed by each quartile, it appears that both the early and mid-early replication quartiles contain a significant fraction of the Spo11-DSBs and the Zip3-ChIP-seq signals, which vary less than twofold between the four quartiles (Fig. 5 *B* and *C*). This shows that the early and mid-early replicated regions from *L. kluyveri* undergo Spo11-DSBs and recombination to a comparable extent as the rest of the genome. Hence, the depletion in Spo11-DSBs and subsequent recombination on Lakl0C-left is not related to its early/mid-early replication timing. Further regulation therefore exists to explain the Spo11-DSBs depletion on Lakl0C-left. Interestingly, the earliest quartile shows slightly fewer Spo11-DSBs than the next two quartiles while it shows slightly more Zip3-ChIP-seq signal, suggesting potential differences in the outcome of early versus late Spo11-DSBs.

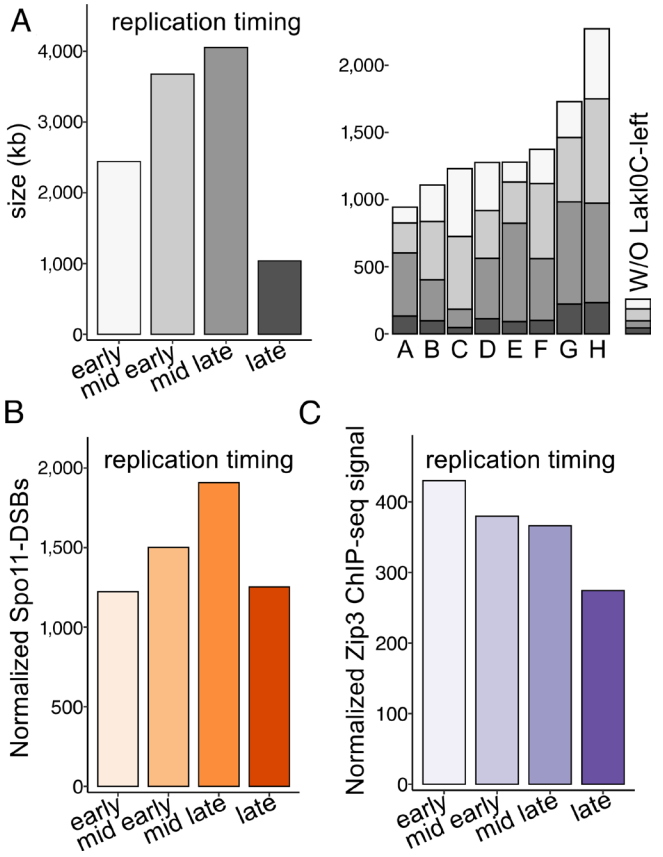

Fig. 5. Spo11-DSBs and Zip3-FLAG ChIP-seq enrichment as a function of the replication timing. (*A*) *L. kluyveri* genome was partitioned in four groups encompassing the entire vegetative replication phase. Each group corresponds to a period of 8 min. The *Left* graph represents the fraction of the genome (in kb) encompassed by each replication group. The *Right* graph represents the fraction of each replication group within each chromosome. W/O Lakl0C-left: region of *L. kluyveri* chromosome C excluding Lakl0C-left. (*B*) Fraction of the Spo11-DSBs signal at 6 h post meiosis induction included in each replication group normalized by the genomic fraction of each group. (*C*) Fraction of the Zip3-FLAG ChIP-seq signal at 6 h post meiosis induction included in each replication group normalized by the genomic fraction of each group.

Lakl0C-left Does Not Synapse. Recombination is required to initiate synaptonemal complex formation and homolog synapsis in *S. cerevisiae* (44). Based on this, the absence of recombination on Lakl0C-left may prevent synapsis in this chromosome arm, unless synaptonemal complex formation and synapsis could spread through its entire length after initiating either right of it or at the very left telomere from which recombination cannot be genetically mapped. To test this prediction, we performed immunofluorescence staining of *L. kluyveri* meiotic chromosome spreads using a *S. cerevisiae* anti-Zip1 antibody that cross-reacts in *L. kluyveri* and an anti-FLAG antibody directed against a FLAG-tagged version of Rec8. Experiments were performed in the absence of Ndt80 to block cells at the pachytene stage. As expected, we observed continuous Zip1 staining of *L. kluyveri* meiotic chromosomes (Fig. 6 *A* and *B*). We observed on average nine Zip1 continuous lines per nucleus in agreement with the chromosome number. Interestingly, the cumulated length of Zip1 lines in *L. kluyveri* is 13.86 micrometers on average compared to 28 micrometers in *S. cerevisiae* (Fig. 6*C*). This ca. twofold longer meiotic chromosome size agrees with the ca. fourfold higher recombination frequency in *S. cerevisiae* compared to *L. kluyveri* (50). It also suggests longer loops in *L. kluyveri* than in *S. cerevisiae*. Measurement of the width of the DAPI signal of pachytene chromosomes spread on the same slide showed this width was on average 1.26 micrometers in *L. kluyveri* and 0.83 micrometers in *S. cerevisiae*, therefore supporting longer chromatin loops in *L. kluyveri* (Fig. 6 *D* and *E*).

Rec8 staining colocalized with Zip1 staining except at two regions that exhibited Rec8-only staining (Fig. 6*F*). One of these regions exhibits a circular structure emanating from a chromosome which corresponds to the rDNA locus as demonstrated by staining with a specific FISH probe. The second region consists of a "V" shape emanating from a base stained by both Zip1 and Rec8. This overall "Y" shape chromosome could be compatible with chromosome C, with the base of the Y corresponding to the synapsed right arm, and the arms of the Y corresponding to the left arms entirely unsynapsed. Corroborating this hypothesis, using FISH probes specific of the left and the right arms of chromosome C, we could detect that the FISH probe specific of the right arm of chromosome C stains a DAPI dense region, while the FISH probe specific of the left arm of chromosome C stains two nearby areas less DAPI dense (Fig. 6*G*). Such signals support synapsed right arms of chromosome C and unsynapsed left arms. Consistently, at 5 h post meiosis induction, the distance law of Lakl0C-left shows a higher probability of contact at longer range (>100 kb) than other chromosome arms, which could reflect the ability of the unsynapsed arm to contact distant regions (Fig. 3*C*). In agreement with the ChIP-seq experiment that revealed the presence of Rec8 along Lakl0C-left and the Hi-C experiment that revealed normal compaction of Lakl0C-left, the Y structure is also entirely

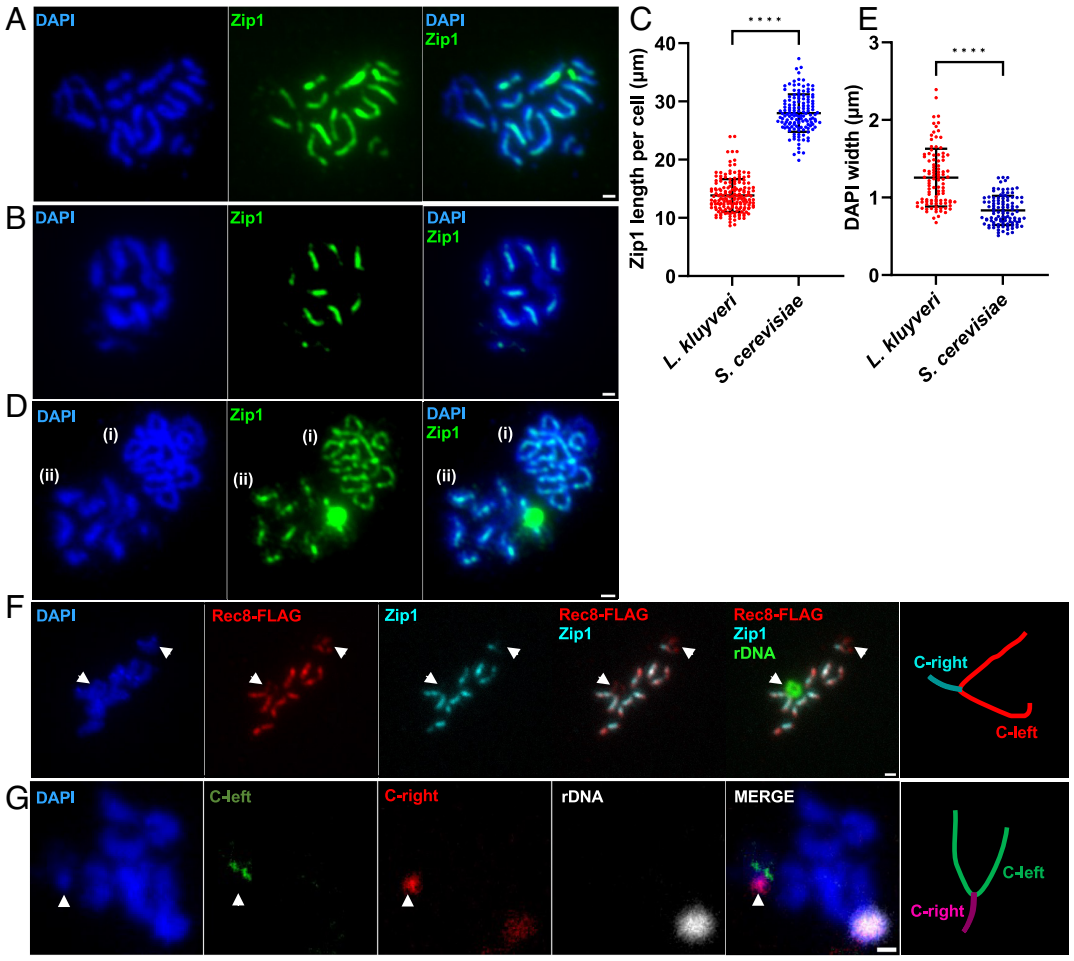

Fig. 6. Cytology of *L. kluyveri* meiotic chromosomes. (*A*) Pachytene spread nuclei of *S. cerevisiae ndt80* mutant strain (BLY1808) 12 h after sporulation induction stained with DAPI (blue) and anti-Zip1 antibody (green). (*B*) Pachytene spread nuclei of *L. kluyveri ndt80* mutant strain (LAKL220) 13.5 h after sporulation induction stained with DAPI (blue) and anti-Zip1 antibody (green). (*C*) Quantification of the total length of Zip1 lines per cell in µm. Black lines show means ± SD. *L. kluyveri:* 13.86 ± 2.81 µm (n = 170), *S. cerevisiae:* 28 ± 3.2 µm (n = 139). The average number of Zip1 lines observed and quantified per cell is 8.7 ± 0.76 for *L. kluyveri* and 14.24 ± 1.32 for *S. cerevisiae.* (*D*) Pachytene spread nuclei of i) *S. cerevisiae ndt80* mutant strain (BLY1808) 12 h after sporulation induction and ii) *L. kluyveri ndt80* mutant strain (LAKL220) 13.5 h after sporulation induction stained with DAPI (blue) and Zip1 (green). *S. cerevisiae* and *L. kluyveri* spread nuclei were mixed on the same slide to make sure they undergo the same treatments. (*E*) Quantification of DAPI signal width from panel *D* which reflects the chromosome loops size. Black lines show mean ± SD. *L. kluyveri:* 1.26 ± 0.37 µm (n = 100), *S. cerevisiae:* 0.83 ± 0.19 µm (n = 104). In panels *C* and *E*, $P < 0.0001$, Mann–Whitney *U* test. (*F* and *G*) Pachytene spread nuclei of *L. kluyveri ndt80* mutant strain (LAKL227) 13.5 h after sporulation induction. In *F*, staining was performed with DAPI (blue), anti-FLAG antibody against Rec8-FLAG (red), anti-Zip1 antibody (cyan) and an rDNA FISH probe (green). The *Left* arrowhead points at the rDNA locus. The *Right* arrowhead points at the inferred chromosome C-left unsynapsed arms. In *G*, staining was performed with DAPI (blue), Lakl0C-left FISH probe (green), Lakl0C-right FISH probe (red), and an rDNA FISH probe (white). The arrowhead points at chromosome C. The structure of chromosome C inferred from staining experiments is drawn (not to scale) on the right of panels *F* and *G*. (Scale bars = 1 µm.)

stained by Rec8. Finally, the fact that the arms of the Y structure are separated further suggests that there is no recombination within the left telomere of chromosome C in regions that could not be genetically mapped nor assessed by our ChIP-seq or CC-seq approaches. Overall, our analysis of *L. kluyveri* meiotic chromosomes spreads reveals that Lakl0C-left does not synapse. This shows that recombination and subsequent synapsis initiated outside Lakl0C-left is not enough to spread through this entire region. Recombination seems therefore also required in *L. kluyveri* to locally initiate homolog synapsis, as in *S. cerevisiae*.

Discussion

The lack of meiotic recombination on Lakl0C-left implies an absolute genetic linkage and an absence of sequence homozygosis by gene conversion during meiosis. This chromosome arm that contains the *MAT* locus therefore relies exclusively on mitotic recombination to break genetic linkages and homogenize mutations. It is therefore expected that Lakl0C-left genes would exhibit a lower purifying selection than the other genes of the genome. This is actually the case, since Lakl0C-left genes show a higher ratio of non-synonymous (dN) to synonymous (dS) substitution rates (dN/dS) than the rest of the genome (80). It is also expected to find a higher density of heterozygous sequence polymorphisms on Lakl0C-left than on the rest of the genome, with at least one possibly being responsible for the different growth phenotypes of *MATa* and *MATα* spores from the CBS10367 isolate. In agreement with this expectation, analysis of the CBS10367 diploid genome with respect to the CBS3082 reference genome revealed a significantly higher fraction of heterozygous SNPs and indels on Lakl0C-left compared to the other chromosomes excluding the highly variable subtelomeric regions, with 1.53 vs. 0.11 heterozygous SNPs per kb and 0.33 vs. 0.018 heterozygous indels per kb, respectively (*SI Appendix*, Table S1 and Fig. S12*A*). Despite this higher SNP density, the most telomeric ca. 200 kb left of chromosome C are almost completely devoid of heterozygous SNPs, potentially reflecting homozygosis by mitotic recombination (G2 crossover or break-induced replication) in the recent history of the strain. Finally, the density of homozygous sequence polymorphisms on Lakl0C-left existing between CBS10367 and CBS3082 is comparable to the

rest of the genome, with 25.29 vs. 23.42 homozygous SNPs per kb, respectively, and is much higher than the density of heterozygous sequence polymorphisms mentioned above (*SI Appendix*, Fig. S12*B*). Given the absence of meiotic recombination on Lakl0C-left that is likely common to all *Lachancea kluyveri* isolates, this suggests a leading role of mitotic recombination in yielding homozygous sequence polymorphisms in *L. kluyveri*.

Having determined the Spo11-DSBs landscape of *L. kluyveri*, we could assess the conservation of the strength of Spo11-DSBs hotspots between *L. kluyveri* and the reference *S. cerevisiae* by comparing the frequency of Spo11-DSBs within syntenic intergenic regions as in ref. 12. The strength of Spo11-DSBs hotspots shows some conservation between *L. kluyveri* and *S. cerevisiae*, with a Pearson correlation coefficient r = 0.63, only slightly smaller than between *S. cerevisiae* and *S. kudriavzevii* (r = 0.68) (12). However, this does not result in conserved crossover hotspots (50). We figured out that the ohnologs provide another relevant dataset to look at the conservation of Spo11-DSBs hotspots within a single genomic environment at a broad evolutionary scale, larger than that of the *Saccharomyces* clade but shorter than that separating *S. cerevisiae* and *L. kluyveri*. Although the sample size is small, the strength of the Spo11-DSBs signal within ohnologous syntenic intergenic regions also shows some conservation (r = 0.37, p = 0.021, 95%CI [0.06, 0.62]). These results extend the evolutionary scale at which the strength of the Spo11-DSB hotspots that do not rely on sequence-specific elements is conserved, the divergence between the *Lachancea* and *Saccharomyces* lineages being older than the 100 million years old *Saccharomyces* lineage-specific whole-genome duplication (81).

In most species studied so far, the number of meiotic crossovers per chromosome is between one and three. *S. cerevisiae* and *S. pombe* are among the outliers with much more crossovers per chromosome (82, 83). With a comparable genome size and twice fewer chromosomes, *L. kluyveri* has ca. four-fold fewer crossovers per meiosis than *S. cerevisiae* (50). *L. kluyveri* therefore resembles most species, with the exception of Lakl0C-left that likely involves an additional mechanism preventing recombination. We observed a ca. two-fold longer synaptonemal complex length in *S. cerevisiae* and a shorter chromosome width as measured by DAPI staining. Given the evolutionary conservation of the dimensions of the "loop-base module" (42) and the similar genome size of *S. cerevisiae* and *L. kluyveri*, this suggests less but longer loops in *L. kluyveri* compared to *S. cerevisiae*. The correlation of chromosome axis length and frequency of crossovers between these two closely related species is reminiscent of the covariation of the frequency of crossovers per nucleus with the chromosome axis length (41, 84). While this latter point suggests a constant crossover frequency per chromatin loop within a given species, the actual crossover frequency per chromatin loop might be different between *L. kluyveri* and *S. cerevisiae*. Overall, given the strong difference in terms of recombination frequency and chromosome axis length between *S. cerevisiae* and *L. kluyveri*, the detailed comparison of their meiotic chromatin loops and associated genes and proteins may be a way to understand what governs the meiotic recombination frequency of a given species. Notably, the Pds5 cohesion maintenance factor and the NuA4 histone acetyltransferase complex catalytic subunit Esa1 were shown to contribute significantly but independently to meiotic chromosome axis length (85, 86). It will be interesting to determine their contributions in the difference in meiotic chromosome axis length between *L. kluyveri* and *S. cerevisiae*.

The Y structure of Lakl0C chromosome during pachytene, with only the base of the Y stained by Zip1, suggests that the synaptonemal complex does not form along Lakl0C-left, although it is present on the right arm of this chromosome. While recombination is essential to initiate synaptonemal complex formation in *S. cerevisiae* and likely in *L. kluyveri* (44), our results suggest that either the extent of polymerization of the synaptonemal complex in *L. kluyveri* is limited and requires initiation points not too far apart to cover chromosomes entirely, and/or that something is specifically inhibiting synaptonemal complex polymerization on Lakl0C-left after its priming outside of Lakl0C-left. Alternatively, the failure to polymerize could be due to the absence of pre-existing Red1 or Hop1, as discussed below.

Our most striking finding is the complete absence of the meiotic axis proteins Hop1 and Red1 from Lakl0C-left. The abundance of these proteins is known to vary along chromosomes. Hop1 is notably enriched in regions with higher recombination activity (16). However, the complete absence of Hop1 and Red1 from a chromosome region that encompasses ca. 8% of the entire genome has not been reported so far, to our knowledge. Despite their phylogenetic divergence, the regulation of meiotic recombination is highly similar between *S. cerevisiae* and *L. kluyveri*. Most, if not all, relevant meiotic recombination genes are conserved between the two species. This contrasts with all the other *Lachancea* species that lost most genes from the ZMM pathway right after the divergence of *L. kluyveri* from the rest of the clade (58, 87). Notably, Hop1, Red1, and Rec8 display similar properties between *S. cerevisiae* and *L. kluyveri*. These include the early recruitment of Rec8 around centromeres and the subsequent recruitment of Rec8 in discrete peaks between convergent genes throughout the genome that strongly colocalize with both Hop1 and Red1 peaks. This suggests conserved recruitment regulation of these proteins. In *S. cerevisiae*, the main Hop1 and Red1 recruitment pathway is through Rec8 that first recruits Red1 which subsequently recruits Hop1 (16, 23). A second recruitment pathway independent of Rec8 and relying on the plant homeodomain (PHD) domain of Hop1 was recently reported (24). The complete absence of both Hop1 and Red1 from Lakl0C-left suggests that these two pathways are inhibited in this entire 1 Mb long region. Whether this relies on the presence of an inhibitory factor, or the absence of an activating factor is so far unknown. Although the specific early replicating profile was a plausible explanation for this chromosome-wide behavior, we showed that other early replication regions are not significantly depleted in Spo11-DSBs and Zip3 ChIP-seq signals. Another hypothesis is that this behavior is related to the ca. 12% higher GC content of Lakl0C-left than the rest of the genome, i.e., 52.9 vs. 40.4% respectively (53, 88). Interestingly, Heldrich et al. (24) showed that the direct recruitment of Hop1 to genomic islands relied on the local DNA sequence. Therefore, one possibility is that Lakl0C-left sequence is incompatible with direct Hop1 recruitment, for reasons that remain to be determined. However, Rec8 is properly loaded on Lakl0C-left as detected by ChIP-seq where it ensures proper chromosome condensation as detected by Hi-C and directly by Rec8 immunostaining. Hence, while the unusual composition bias of Lakl0C-left could explain the absence of direct recruitment of Hop1, it likely does not explain the inhibition of Hop1 recruitment by Rec8.

Extensive recombination suppression is seen on sex chromosomes, self-incompatibility loci in plants and mating type loci in fungi and algae (48). In the case of fungi, the rationale for the initial recombination suppression at the mating type loci is probably to avoid breaking linkage between genes controlling correct mating. In the budding yeasts *S. cerevisiae* and *L. kluyveri*, such genes include *MAT ALPHA1* and *ALPHA2* genes in the Matα genotype, and *MATA1* and *MATA2* in the Mata genotype, although no known role of *MATA2* has been determined so far. Interestingly, recombination cessation extends beyond the *MAT* locus in many fungi, but the selective advantage is not always clear (48). In the case of *L. kluyveri*, the recombination cessation is likely concomitant with the introgression of Lakl0C-left, therefore

relatively recent and includes only one evolutionary stratum covering 80% of chromosome C. No such recombination inhibition is observed in neighbor species including *L. waltii* and *S. cerevisiae*. Interestingly, although meiotic recombination is inhibited, the accumulation of homozygous sequence polymorphisms between isolates suggests that mitotic recombination is taking place equally in Lakl0C-left and the rest of the genome, and that it plays the major role in *L. kluyveri* genome evolution. Overall, while no clear selective advantage has been identified so far for the recombination cessation on Lakl0C-left, the mechanism reported here, i.e., the lack of recruitment of meiotic chromosome axis proteins, could be responsible for the extension of recombination cessation around mating type loci in many fungal genomes and play an important role in the emergence of sex chromosomes that rely on the cessation of meiotic recombination (48, 89).

Summary of Materials and Methods

See *SI Appendix* for a complete description of the materials and methods.

Strains and Media. All yeast strains used in this study are derivatives of *L. kluyveri* CBS10367 natural diploid isolate (54). Strain genotypes are listed in *SI Appendix*, Table S2 as well as plasmids used. Gene editing was performed by PCR-mediated gene targeting followed by PCR analysis as described in (50). Oligonucleotides are listed in *SI Appendix*, Table S3.

L. kluyveri meiotic progression is rather fast and synchronous (*SI Appendix*, Fig. S6*A*), and shows between 1 and 2 h of delay compared to the *S. cerevisiae* reference SK1 isolate (50). The 4- and 6-h time points post meiosis induction used for ChIP-seq experiments roughly correspond to the beginning and the end of meiotic prophase for most cells of the population. The 13.5-h time point post meiosis induction is specific to *ndt80* mutant cells to ensure most cells are pachytene arrested.

CBS10367 Genome Sequencing. CBS10367 genome was sequenced at BGI. Reads were mapped to the *L. kluyveri* CBS3082 reference genome to infer the CBS10367 complete genome sequence from the homozygous SNPs and indels. This yielded the CBS10367_SNP_inferred and CBS10367_SNP_indels_inferred genome sequences (details in *SI Appendix*).

CC-seq Experiments and Data Analysis. The *sae2* strain LAKL 221 was used to perform meiotic time courses. CC-seq experiments were performed 6 h after meiosis induction, which corresponds to the peak of Spo11-DSBs (50), following the procedure described in ref. 56 but with 10 times more cells and mechanical cell lysis. Sequences were analyzed as in ref. 56 using *L. kluyveri* CBS10367_SNP_inferred as a reference genome and empirically removing the high background signal (details in *SI Appendix*).

Onholog Analysis. Spo11-DSB counts of S288C *S. cerevisiae* strain were extracted from (10) supp data "FullMap.Spo11.S288C_chrX.txt". The sum of the DSBs within intergenic regions was determined using the S288C reference genome (https://www.yeastgenome.org, downloaded March 2023). Pairs of syntenic intergenic regions flanked by ohnologs were identified with the list available at http://wolfe.gen.tcd.ie/ygob (60).

ChIP-seq experiments and data analysis. ChIP-seq experiments were performed and analyzed as in refs. 47 and 90 (details in *SI Appendix*). All immunoprecipitations used the mouse anti-FLAG M2 antibody (Sigma). The expression of the FLAG-tagged proteins was verified by western blotting (*SI Appendix*, Fig. S5). ChIP-sequencing was performed with a Hiseq2500 sequencer (Illumina) using a 50-nt paired-end protocol. Two independent replicates of each condition were analyzed except for Zip3-FLAG that contained five replicates (*SI Appendix*, Fig. S7). All sequencing data were visualized using the Integrative Genomics Viewer (IGV; v2.5.2) (91).

Hi-C. Hi-C experiments were performed on meiotic cultures with the Arima Hi-C kit (Arima Genomics; restriction: DpnII, HinfI). Hi-C DNA libraries were performed as described in ref. 92 and paired-end sequenced on an Illumina NextSeq500 system (2 × 35 bp). Processing of the contact data was done with Hicstuff pipeline on the CBS10367_SNP_inferred reference genome (93) (details in *SI Appendix*).

Meiotic Chromosome Spreads, Immunostaining, and Image Acquisition. Chromosome spreads from meiotic cultures were prepared following the protocol described in ref. 94 with some modifications. Slides with spread nuclei were sequentially incubated with the proper primary and secondary antibodies. Primary antibodies were affinity-purified rabbit anti-*S. cerevisiae* Zip1 antibody (Gift from A. MacQueen, dilution 1:100), and mouse monoclonal anti-FLAG primary antibody M2 (Sigma, dilution 1:300). FISH probes were generated using the nick-translation kit from Abbott Molecular using CF dye-conjugated dUTP (Biotium), on a pool of PCR products of about 6-kb-long except for the rDNA probe where a single 8-kb-long PCR product was used. Fluorescence microscopy was performed on a ZEISS IMAGER Z2 upright microscope. The measurements of chromosome axis length and DAPI width were done manually as described in ref. 85. The distinctive "V"-shaped structure was identified in every complete pachytene chromosome spread analyzed. Complete pachytene spreads correspond to those displaying all eight homologous chromosome pairs. This pattern was identified in over 100 spreads examined through various experiments utilizing DAPI and Zip1 staining, and those utilizing DAPI, Zip1, and Rec8 staining. In the cases presented in Fig. 6 *F* and *G*, the FISH signals were confirmed in 8 and 10 spreads, respectively, that corresponded to all the interpretable spreads for these specific experiments.

Data, Materials, and Software Availability. The Illumina reads related to the CBS10367 whole-genome sequencing are available in the Sequence Read Archive under the BioProject PRJEB60460 (95). The CC-seq, ChIP-seq, and Hi-C data discussed in this publication have been deposited in NCBI's Gene Expression Omnibus (96) and are accessible through GEO SuperSeries accession number GSE237708 (https://www.ncbi.nlm.nih.gov/geo/query/acc.cgi?acc=GSE237708). All other data are included in the manuscript and/or *SI Appendix*.

ACKNOWLEDGMENTS. We thank Alexandra Pyatnitskaya for her support to the chromosome-spreading technique and Samuel Granjeaud for his support in statistics. We thank Amy MacQueen for the gift of the anti-Zip1 antibody, and Valérie Garcia and Marie Dorme for the gift of the *S. cerevisiae* BLY1808 strain. We thank our CRCM colleagues Valérie Garcia, Cédric Giaccherini, Jean-Hugues Guervilly, and Mauro Modesti for fruitful discussions. This research was funded in whole or in part by the Wellcome Trust. For the purpose of Open Access, the author has applied a CC BY public copyright license to any Author Accepted Manuscript (AAM) version arising from this submission.

Author affiliations: [a]Centre de recherche en cancérologie de Marseille, CNRS UMR 7258, INSERM, Aix Marseille Université, Institut Paoli Calmettes, Marseille 13009, France; [b]Institut Pasteur, CNRS UMR 3525, Université Paris Cité, Unité Régulation Spatiale des Génomes, Paris 75015, France; [c]Institut Curie, Paris Sciences and Lettres University, Sorbonne Université, CNRS UMR 3244, Dynamics of Genetic Information, Paris 75005, France; [d]Genome Damage and Stability Centre, School of Life Sciences, University of Sussex, Brighton BN1 9RH, United Kingdom; and [e]Université de Strasbourg, CNRS, Génétique moléculaire, génomique, microbiologie UMR 7156, Strasbourg 67000, France

Author contributions: S.L., A. Saifudeen, H.B., A.F., J.S., M.J.N., V.B., R.K., and B.L. designed research; S.L., A. Saifudeen, H.B., A.B., A.T., L.A., M.G., A. Sanchez, and D.J. performed research; S.L., A. Saifudeen, H.B., J.V., A.G., A.T., L.A., A.F., J.S., M.J.N., V.B., R.K., and B.L. analyzed data; and S.L. and B.L. wrote the paper.

1. L. Cao, E. Alani, N. Kleckner, A pathway for generation and processing of double-strand breaks during meiotic recombination in *S. cerevisiae*. *Cell* **61**, 1089–1101 (1990).
2. A. Nicolas, D. Treco, N. P. Schultes, J. W. Szostak, An initiation site for meiotic gene conversion in the yeast *Saccharomyces cerevisiae*. *Nature* **338**, 35–39 (1989).
3. H. Sun, D. Treco, N. P. Schultes, J. W. Szostak, Double-strand breaks at an initiation site for meiotic gene conversion. *Nature* **338**, 87–90 (1989).
4. A. Bergerat *et al.*, An atypical topoisomerase II from archaea with implications for meiotic recombination. *Nature* **386**, 414–417 (1997).
5. C. Claeys Bouuaert *et al.*, DNA-driven condensation assembles the meiotic DNA break machinery. *Nature* **592**, 144–149 (2021).
6. C. Claeys Bouuaert *et al.*, Structural and functional characterization of the Spo11 core complex. *Nat. Struct. Mol. Biol.* **28**, 92–102 (2021).

7. S. Keeney, C. N. Giroux, N. Kleckner, Meiosis-specific DNA double-strand breaks are catalyzed by Spo11, a member of a widely conserved protein family. *Cell* **88**, 375–384 (1997).
8. S. Maleki, M. J. Neale, C. Arora, K. A. Henderson, S. Keeney, Interactions between Mei4, Rec114, and other proteins required for meiotic DNA double-strand break formation in *Saccharomyces cerevisiae*. *Chromosoma* **116**, 471–486 (2007).
9. F. Baudat, A. Nicolas, Clustering of meiotic double-strand breaks on yeast chromosome III. *Proc. Natl. Acad. Sci. U.S.A.* **94**, 5213–5218 (1997).
10. J. Pan *et al.*, A hierarchical combination of factors shapes the genome-wide topography of yeast meiotic recombination initiation. *Cell* **144**, 719–731 (2011).
11. T. D. Petes, Meiotic recombination hot spots and cold spots. *Nat. Rev. Genet* **2**, 360–369 (2001).
12. I. Lam, S. Keeney, Nonparadoxical evolutionary stability of the recombination initiation landscape in yeast. *Science* **350**, 932–937 (2015).
13. Y. Blat, R. U. Protacio, N. Hunter, N. Kleckner, Physical and functional interactions among basic chromosome organizational features govern early steps of meiotic chiasma formation. *Cell* **111**, 791–802 (2002).
14. P. B. Møens, R. E. Pearlman, Chromatin organization at meiosis. *BioEssays* **9**, 151–153 (1988).
15. H. Muller *et al.*, Characterizing meiotic chromosomes' structure and pairing using a designer sequence optimized for Hi-C. *Mol. Syst. Biol.* **14**, e8293 (2018).
16. S. Panizza *et al.*, Spo11-accessory proteins link double-strand break sites to the chromosome axis in early meiotic recombination. *Cell* **146**, 372–383 (2011).
17. S. A. Schalbetter, G. Fudenberg, J. Baxter, K. S. Pollard, M. J. Neale, Principles of meiotic chromosome assembly revealed in *S. cerevisiae*. *Nat. Commun.* **10**, 4795 (2019).
18. D. Zickler, N. Kleckner, Meiotic chromosomes: Integrating structure and function. *Annu. Rev. Genet.* **33**, 603–754 (1999).
19. N. M. Hollingsworth, L. Goetsch, B. Byers, The *HOP1* gene encodes a meiosis-specific component of yeast chromosomes. *Cell* **61**, 73–84 (1990).
20. F. Klein *et al.*, A central role for cohesins in sister chromatid cohesion, formation of axial elements, and recombination during yeast meiosis. *Cell* **98**, 91–103 (1999).
21. A. V. Smith, G. S. Roeder, The yeast Red1 protein localizes to the cores of meiotic chromosomes. *J. Cell Biol.* **136**, 957–967 (1997).
22. A. M. West *et al.*, A conserved filamentous assembly underlies the structure of the meiotic chromosome axis. *eLife* **8**, e40372 (2019).
23. X. Sun *et al.*, Transcription dynamically patterns the meiotic chromosome-axis interface. *eLife* **4**, e07424 (2015).
24. J. Heldrich *et al.*, Two pathways drive meiotic chromosome axis assembly in *Saccharomyces cerevisiae*. *Nucleic Acids Res.* **50**, 4545–4556 (2022).
25. L. Acquaviva *et al.*, The COMPASS subunit Spp1 links histone methylation to initiation of meiotic recombination. *Science* **339**, 215–218 (2013).
26. Y. Mao-Draayer, A. M. Galbraith, D. L. Pittman, M. Cool, R. E. Malone, Analysis of meiotic recombination pathways in the yeast *Saccharomyces cerevisiae*. *Genetics* **144**, 71–86 (1996).
27. H. Murakami *et al.*, Multilayered mechanisms ensure that short chromosomes recombine in meiosis. *Nature* **582**, 124–128 (2020).
28. A. Peciña *et al.*, Targeted stimulation of meiotic recombination. *Cell* **111**, 173–184 (2002).
29. V. Sommermeyer, C. Béneut, E. Chaplais, M. E. Serrentino, V. Borde, Spp1, a member of the Set1 Complex, promotes meiotic DSB formation in promoters by tethering histone H3K4 methylation sites to chromosome axes. *Mol. Cell* **49**, 43–54 (2013).
30. D. Woltering *et al.*, Meiotic segregation, synapsis, and recombination checkpoint functions require physical interaction between the chromosomal proteins Red1p and Hop1p. *Mol. Cell Biol.* **20**, 6646–6658 (2000).
31. L. Xu, B. M. Weiner, N. Kleckner, Meiotic cells monitor the status of the interhomolog recombination complex. *Genes Dev.* **11**, 106–118 (1997).
32. K. Kugou *et al.*, Rec8 guides canonical Spo11 distribution along yeast meiotic chromosomes. *Mol. Biol. Cell* **20**, 3064–3076 (2009).
33. V. Garcia, S. E. L. Phelps, S. Gray, M. J. Neale, Bidirectional resection of DNA double-strand breaks by Mre11 and Exo1. *Nature* **479**, 241–244 (2011).
34. M. J. Neale, J. Pan, S. Keeney, Endonucleolytic processing of covalent protein-linked DNA double-strand breaks. *Nature* **436**, 1053–1057 (2005).
35. A. Schwacha, N. Kleckner, Identification of joint molecules that form frequently between homologs but rarely between sister chromatids during yeast meiosis. *Cell* **76**, 51–63 (1994).
36. A. Schwacha, N. Kleckner, Interhomolog bias during meiotic recombination: Meiotic functions promote a highly differentiated interhomolog-only pathway. *Cell* **90**, 1123–1135 (1997).
37. S. L. Page, R. S. Hawley, The genetics and molecular biology of the synaptonemal complex. *Annu. Rev. Cell Dev. Biol.* **20**, 525–558 (2004).
38. C. K. Cahoon, R. S. Hawley, Regulating the construction and demolition of the synaptonemal complex. *Nat. Struct. Mol. Biol.* **23**, 369–377 (2016).
39. C. Chen, A. Jomaa, J. Ortega, E. E. Alani, Pch2 is a hexameric ring ATPase that remodels the chromosome axis protein Hop1. *Proc. Natl. Acad. Sci. U.S.A.* **111**, E44–E53 (2014).
40. V. V. Subramanian *et al.*, Chromosome synapsis alleviates Mek1-dependent suppression of meiotic DNA repair. *PLoS Biol.* **14**, e1002369 (2016).
41. N. Kleckner, A. Storlazzi, D. Zickler, Coordinate variation in meiotic pachytene SC length and total crossover/chiasma frequency under conditions of constant DNA length. *Trends Genet.* **19**, 623–628 (2003).
42. N. Kleckner, Chiasma formation: Chromatin/axis interplay and the role(s) of the synaptonemal complex. *Chromosoma* **115**, 175–194 (2006).
43. A. Lynn, R. Soucek, G. V. Börner, ZMM proteins during meiosis: Crossover artists at work. *Chromosome Res.* **15**, 591–605 (2007).
44. A. Pyatnitskaya, V. Borde, A. De Muyt, Crossing and zipping: Molecular duties of the ZMM proteins in meiosis. *Chromosoma* **128**, 181–198 (2019).
45. S. Agarwal, G. S. Roeder, Zip3 provides a link between recombination enzymes and synaptonemal complex proteins. *Cell* **102**, 245–255 (2000).
46. M.-E. Serrentino, E. Chaplais, V. Sommermeyer, V. Borde, Differential association of the conserved SUMO ligase Zip3 with meiotic double-strand break sites reveals regional variations in the outcome of meiotic recombination. *PLoS Genet.* **9**, e1003416 (2013).
47. A. De Muyt *et al.*, A meiotic XPF–ERCC1-like complex recognizes joint molecule recombination intermediates to promote crossover formation. *Genes Dev.* **32**, 283–296 (2018).
48. F. E. Hartmann *et al.*, Recombination suppression and evolutionary strata around mating-type loci in fungi: Documenting patterns and understanding evolutionary and mechanistic causes. *New Phytol.* **229**, 2470–2491 (2021).
49. D. Charlesworth, Evolution of recombination rates between sex chromosomes. *Philos. Trans. R Soc. Lond. B Biol. Sci.* **372**, 20160456 (2017).
50. C. Brion *et al.*, Variation of the meiotic recombination landscape and properties over a broad evolutionary distance in yeasts. *PLoS Genet.* **13**, e1006917 (2017).
51. C. Kurtzman, Phylogenetic circumscription of *Saccharomyces*, *Kluyveromyces* and other members of the *Saccharomycetaceae*, and the proposal of the new genera *Lachancea*, *Nakaseomyces*, *Naumovia, Vanderwaltozyma and Zygotorulaspora*. *FEMS Yeast Res.* **4**, 233–245 (2003).
52. P. Cliften *et al.*, Finding functional features in *Saccharomyces* genomes by phylogenetic footprinting. *Science* **301**, 71–76 (2003).
53. J.-L. Souciet *et al.*; Génolevures Consortium, Comparative genomics of protoploid Saccharomycetaceae. *Genome Res.* **19**, 1696–1709 (2009).
54. A. Friedrich, P. Jung, C. Reisser, G. Fischer, J. Schacherer, Population genomics reveals chromosome-scale heterogeneous evolution in a protoploid yeast. *Mol. Biol. Evol.* **32**, 184–192 (2015).
55. N. Agier, O. M. Romano, F. Touzain, M. Cosentino Lagomarsino, G. Fischer, The Spatiotemporal Program of Replication in the Genome of *Lachancea kluyveri*. *Genome Biol. Evol.* **5**, 370–388 (2013).
56. W. H. Gittens *et al.*, A nucleotide resolution map of Top2-linked DNA breaks in the yeast and human genome. *Nat. Commun.* **10**, 4846 (2019).
57. Y. Zhang *et al.*, Model-based analysis of ChIP-Seq (MACS). *Genome Biol.* **9**, R137 (2008).
58. N. Vakirlis *et al.*, Reconstruction of ancestral chromosome architecture and gene repertoire reveals principles of genome evolution in a model yeast genus. *Genome Res.* **26**, 918–932 (2016).
59. S. Ohno, *Evolution by Gene Duplication*, S. Ohno, Ed. (Springer_Verlag, 1970).
60. K. P. Byrne, K. H. Wolfe, The yeast gene order browser: Combining curated homology and syntenic context reveals gene fate in polyploid species. *Genome Res.* **15**, 1456–1461 (2005).
61. C. Brion, C. Caradec, D. Pflieger, A. Friedrich, J. Schacherer, Pervasive phenotypic impact of a large nonrecombining introgressed region in yeast. *Mol. Biol. Evol.* **37**, 2520–2530 (2020).
62. B. D. Harfe, S. Jinks-Robertson, DNA mismatch repair and genetic instability. *Annu. Rev. Genet.* **34**, 359–399 (2000).
63. N. Hunter, S. R. Chambers, E. J. Louis, R. H. Borts, The mismatch repair system contributes to meiotic sterility in an interspecific yeast hybrid. *EMBO J.* **15**, 1726–1733 (1996).
64. E. Martini *et al.*, Genome-wide analysis of heteroduplex DNA in mismatch repair-deficient yeast cells reveals novel properties of meiotic recombination pathways. *PLoS Genet.* **7**, e1002305 (2011).
65. E. Lieberman-Aiden *et al.*, Comprehensive mapping of long-range interactions reveals folding principles of the human genome. *Science* **326**, 289–293 (2009).
66. G. A. Brar *et al.*, Rec8 phosphorylation and recombination promote the step-wise loss of cohesins in meiosis. *Nature* **441**, 532–536 (2006).
67. A. Lengronne *et al.*, Cohesin relocation from sites of chromosomal loading to places of convergent transcription. *Nature* **430**, 573–578 (2004).
68. C. Matthey-Doret *et al.*, Computer vision for pattern detection in chromosome contact maps. *Nat. Commun.* **11**, 5795 (2020).
69. J.-L. Souciet *et al.*, Comparative genomics of protoploid *Saccharomycetaceae*. *Genome Res.* **19**, 1696–1709 (2009).
70. J. M. Bailis, G. S. Roeder, Synaptonemal complex morphogenesis and sister-chromatid cohesion require Mek1-dependent phosphorylation of a meiotic chromosomal protein. *Genes Dev.* **12**, 3551–3563 (1998).
71. H. Niu *et al.*, Partner choice during meiosis is regulated by Hop1-promoted dimerization of Mek1. *Mol Biol Cell* **16**, 5804–5818 (2005).
72. A. Shodhan, M. Xaver, D. Wheeler, M. Lichten, Turning coldspots into hotspots: Targeted recruitment of axis protein Hop1 stimulates meiotic recombination in Saccharomyces cerevisiae. *Genetics* **222**, iyac106 (2022).
73. J. Lange *et al.*, The landscape of mouse meiotic double-strand break formation, processing, and repair. *Cell* **167**, 695–708.e16 (2016).
74. A. Lukaszewicz, J. Lange, S. Keeney, M. Jasin, De novo deletions and duplications at recombination hotspots in mouse germlines. *Cell* **184**, 5970–5984.e18 (2021).
75. D. Johnson *et al.*, Concerted cutting by Spo11 illuminates meiotic DNA break mechanics. *Nature* **594**, 572–576 (2021).
76. H. G. Blitzblau, A. Hochwagen, ATR/Mec1 prevents lethal meiotic recombination initiation on partially replicated chromosomes in budding yeast. *eLife* **2**, e00844 (2013).
77. H. Murakami, S. Keeney, Temporospatial coordination of meiotic DNA replication and recombination via DDK recruitment to replisomes. *Cell* **158**, 861–873 (2014).
78. V. Borde, A. S. H. Goldman, M. Lichten, Direct coupling between meiotic DNA replication and recombination initiation. *Science* **290**, 806–809 (2000).
79. N. Agier *et al.*, The evolution of the temporal program of genome replication. *Nat. Commun.* **9**, 2199 (2018).
80. C. Brion, D. Pflieger, A. Friedrich, J. Schacherer, Evolution of intraspecific transcriptomic landscapes in yeasts. *Nucleic Acids Res.* **43**, 4558–4568 (2015).
81. K. H. Wolfe, D. C. Shields, Molecular evidence for an ancient duplication of the entire yeast genome. *Nature* **387**, 708–713 (1997).
82. R. Mercier, C. Mézard, E. Jenczewski, N. Macaisne, M. Grelon, The molecular biology of meiosis in plants. *Annu. Rev. Plant Biol.* **66**, 297–327 (2015).
83. Q. Lian, L. Maestroni, M. Gaudin, B. Llorente, R. Mercier, Meiotic recombination is confirmed to be unusually high in the fission yeast *Schizosaccharomyces pombe*. *iScience* **26**, 107614 (2023).
84. S. Wang *et al.*, Per-nucleus crossover covariation and implications for evolution. *Cell* **177**, 326–338. e16 (2019).
85. M. Song *et al.*, Interplay between Pds5 and Rec8 in regulating chromosome axis length and crossover frequency. *Sci. Adv.* **7**, eabe7920 (2021).
86. Y. Wang *et al.*, ESA1 regulates meiotic chromosome axis and crossover frequency via acetylating histone H4. *Nucleic Acids Res.* **49**, 9353–9373 (2021).
87. F. Dutreux *et al.*, Lessons from the meiotic recombination landscape of the ZMM deficient budding yeast *Lachancea waltii*. *PLoS Genet.* **19**, e1010592 (2023).
88. C. Payen *et al.*, Unusual composition of a yeast chromosome arm is associated with its delayed replication. *Genome Res.* **19**, 1710–1721 (2009).
89. S. Ponnikas, H. Sigeman, J. K. Abbott, B. Hansson, Why do sex chromosomes stop recombining? *Trends Genet.* **34**, 492–503 (2018).

90. A. Sanchez, V. Borde, Methods to map meiotic recombination proteins in Saccharomyces cerevisiae. *Methods Mol. Biol.* **2153**, 295–306 (2021).
91. J. T. Robinson *et al.*, Integrative genomics viewer. *Nat. Biotechnol.* **29**, 24–26 (2011).
92. L. Dauban *et al.*, Regulation of cohesin-mediated chromosome folding by Eco1 and other partners. *Mol. Cell* **77**, 1279–1293.e4 (2020).
93. C. Matthey-Doret *et al.*, "Normalization of chromosome contact maps: Matrix balancing and visualization" in *Hi-C Data Analysis*, Methods in Molecular Biology, S. Bicciato, F. Ferrari, Eds. (Springer, US, 2022), pp. 1–15.
94. J. Grubb, M. S. Brown, D. K. Bishop, Surface spreading and immunostaining of yeast chromosomes. *J. Vis. Exp.*, **102**, e53081 (2015).
95. A. Friedrich, J. Schacherer, "Sequencing of Lachancea kluyveri, CBS10367 isolate". European Nucleotide Archive. https://www.ebi.ac.uk/ena/browser/view/PRJEB60460. Deposited 7 March 2023.
96. R. Edgar, M. Domrachev, A. E. Lash, Gene expression omnibus: NCBI gene expression and hybridization array data repository. *Nucleic Acids Res.* **30**, 207–210 (2002).